Chemical Science

ROYAL SOCIETY OF CHEMISTRY

EDGE ARTICLE

View Article Online
View Journal | View Issue

Cite this: *Chem. Sci.*, 2024, **15**, 15913

All publication charges for this article have been paid for by the Royal Society of Chemistry

Quantifying variation in cooperative B–H bond activations using Os(II) and Os(III) κ^2-*N*,*S*-chelated complexes: same, but different†

Sourav Gayen, Faneesha Assanar, Sampad Shyamal, Dorothy Priyanka Dorairaj and Sundargopal Ghosh *

In an effort to investigate small molecule activation by heavier transition metal (TM) based κ^2-*N*,*S*-chelated species, we have synthesised a series of bis-κ^2-1,3-*N*,*S*-chelated complexes of osmium, $[Os(PPh_3)_2(\kappa^2\text{-}N,S\text{-}L^a/L^b)_2]$, **2a–b**, and $[Os(PPh_3)(L^a/L^b)(\kappa^2\text{-}N,S\text{-}L^a/L^b)_2]$, **3a–b** (**2a** and **3a**: L^a = $C_7H_4NS_2$; **2b** and **3b**: L^b = C_5H_4NS), from the thermolysis of $[Os(PPh_3)_3Cl_2]$, **1**, with a potassium salt of heterocyclic ligands L^a and L^b. The former complexes are diamagnetic in nature, while the EPR spectra, XPS study and density functional theory (DFT) calculations have substantiated the paramagnetic behaviour of **3a–b** with a significant spin contribution from non-innocent ligands. These species were engaged in B–H activation of boranes utilizing the combined effect of hemilability and metal–ligand cooperativity (MLC), where **2a–b** upon treatment with $BH_3{\cdot}SMe_2$ yielded Os(σ-borate)hydride complexes, $[Os(PPh_3)_2(H)\{\kappa^3\text{-}H,S,S'\text{-}BH_2(L^a/L^b)_2\}]$, **4a–b** (**4a**: L^a = $C_7H_4NS_2$; **4b**: L^b = C_5H_4NS). The formation of **4a–b** was emphasized on the basis of possible dual B–H activation that involved a few concerted steps, *i.e.*, (i) cleavage of one hemilabile Os–N bond and cooperative B–H bond activation, (ii) cleavage of another hemilabile Os–N bond and formation of a B–N bond and (iii) activation of another B–H bond. In stark contrast, the paramagnetic bis-κ^2-1,3-*N*,*S*-chelated species **3a–b** manifested diverse activation patterns in the light of the different electronic nature of non-innocent ligands. While the reaction of **3b** with borane generated dihydridoborate species, $[Os(PPh_3)(\kappa^2\text{-}N,S\text{-}L^b)(\kappa^3\text{-}H,H,S'\text{-}BH_2(OH)C_5H_4NS)]$, **5**, complex **3a** led to the formation of an Os(σ-borate) complex, $[Os(PPh_3)(\kappa^2\text{-}N,S\text{-}L^a)(\kappa^3\text{-}H,S,S'\text{-}BH_2L_2{}^a)]$, *trans*-**6**. As the σ-borate entity shows a tendency to adapt to different spatial arrangements around the metal center, we have established a modified synthetic strategy to isolate the *cis* isomer of **6** that involved the reaction of $[Os(PPh_3)_3Cl_2]$, **1**, with $NaBH_2L^a{}_2$. In a similar fashion, the treatment of $[Os(PPh_3)_3Cl_2]$, **1**, with $NaBH_2L^b{}_2$ yielded $[Os(PPh_3)(\kappa^2\text{-}N,S\text{-}L^b)(\kappa^3\text{-}H,S,S'\text{-}BH_2L_2{}^b)]$, *cis*-**7**. The kinetic and thermodynamic stability of these isomeric species were investigated on the basis of extensive density functional theory (DFT) calculations. Theoretical calculations also provided insightful information on the electronic nature of the species, generated from B–H activations of boranes.

Received 30th July 2024
Accepted 16th August 2024

DOI: 10.1039/d4sc05092d

rsc.li/chemical-science

Introduction

Metal–ligand cooperation (MLC), the synergistic interplay between a metal and ligand, plays a dominant role in the catalytic activation of small molecules.[1,2] While classical catalysis involves solely metal-based catalytic activity, ligands in cooperative transition metal architectures concertedly participate in the cleavage or formation of inert chemical bonds. In particular, the activation of H–H, C–H, N–H, O–H, B–H and Si–H bonds has been extensively studied utilizing MLC.[3–6] Thus, these representatives evolved as privileged catalysts in various catalytic processes, such as hydrogenation, borylation, hydroboration, hydrosilylation, *etc.*[7,8] Conceptually, these species can be better defined as a hybrid molecular architecture by incorporating a transition metal as one of the components in Frustrated Lewis Pairs (FLPs), often termed transition metal frustrated Lewis pairs (TMFLPs).[9] The molecular control over the bond activation process can be implemented by tuning the transition metal as well as modulating the steric and electronic properties of ligand scaffolds, thus resulting in a polarized hybrid platform. Based on the metal–ligand combination, these types of polarized systems can be differentiated into two categories; (i) electron-donating metal (LB)–electron-accepting

Department of Chemistry, Indian Institute of Technology Madras, Chennai 600036, India. E-mail: sghosh@iitm.ac.in

† Electronic supplementary information (ESI) available. CCDC 2353030 (for **2b**), 2353031 (for **4a**), 2353032 (for **5**), 2353033 (for *trans*-**6**), 2353034 (for *cis*-**6**) and 2353035 (for *cis*-**7**) contain the supplementary crystallographic data for this paper. For ESI and crystallographic data in CIF or other electronic format see DOI: https://doi.org/10.1039/d4sc05092d

ligand (LA) and (ii) electron-accepting metal (LA)–electron-donating ligand (LB).[10]

In the recent past, significant progress has been made in E–H (E = H, B, Si, C) bond activation utilizing a cooperative design, comprising an electron-accepting metal centre and electron-donating functionality. For example, Oestreich and co-workers extensively studied the heterolytic activation of the E–H bond across the Ru–S bond of a tethered ruthenium thiolate complex that generates a metal hydride and sulphur stabilized E^+ cation, **I** (Chart 1).[3b,d,11] As per the reports of the Gessner group, a methandiide derived carbene complex of ruthenium was engaged in the activation of several small molecules, *e.g.* hydrogen, silanes, phosphines and phosphine oxides, where protonation took place in the carbonic carbon atom (**II**, Chart 1).[3c,12,13] In contrast, a versatile pattern of activation was investigated in the case of complexes of palladium, which successfully cleaved E–H (E= B, Si) bonds to generate hydrido derivatives, **III**, while treating with Ph_3SiH and germanes, possessing high acidity, led to the formation of silyl and germyl complexes, respectively.[4a] Interestingly, Casey and Clark isolated silyloxy and boroxycyclopentadienyl hydrido–ruthenium complexes, **IV**, by the heterolytic cleavage of Si–H and B–H bonds, respectively, using dimeric ruthenium species.[14] Apart from other small molecules, hydroboranes exhibit peculiarities due to the high electropositivity of boron and the hydridic nature of bound hydrogens. In this context, Drover, Schafer and Love demonstrated the activation of hindered borane, $HBCy_2$, employing the hemilability and joint metal–ligand cooperativity of κ^2-*N*,*O* chelated phosphoramidate complexes of group-9 TM (**V**).[15] Similarly, Stradiotto reported that a κ^2-*P*,*O* chelated phosphino enolate complex of ruthenium promoted the insertion of H_2BMes by the cleavage of the Ru–O bond, affording a dihydridoborate complex, **VI**.[16] Daly and co-workers demonstrated the electrochemical behaviour of a redox-active ruthenium complex, **VII**, in which two BH_3 units encountered cooperative binding along the Ru–N bond.[17] It is worth noting that the field of MLC has recently evolved by introducing heavier main group elements into the ligand scaffold.[18] However, the influence of heavier transition metals as cooperative partners in MLC is less explored.

In the course of our recent studies, we have engaged a series of transition metal based κ^2-*N*,*S*-chelated complexes in the cooperative activation of various small molecules, such as hydroboranes, hydrosilanes, alkynes and $GeCl_2$.[19,20] The combination of hard (N) and soft (S) centres in polydentate ligands offered the activation of E-H (E = B, Si or C) bonds by the cleavage of M–X (X = N, S) bonds. Notably, the activation of boranes yielded TM σ-borate species,[19a,b,20a] featuring M–H–B interactions. For instance, a redox-active ruthenium system was engaged in unusual dual side B–H activation of H_2BMes that resulted in the formation of Ru-bis(dihydridoborate) species, **VIII**.[19b] Building on our previous studies, we have sought to explore the activation chemistry of osmium, a heavier group-8 TM based κ^2-*N*,*S*-chelated species. In this context, we have synthesized two different types of κ^2-*N*,*S*-chelated osmium complexes, diamagnetic $[Os(PPh_3)_2\{\kappa^2\text{-}N,S\text{-}(L^a/L^b)\}_2]$, **2a–b**, and paramagnetic $[Os(PPh_3)(L^a/L^b)(\kappa^2\text{-}N,S\text{-}L^a/L^b)_2]$, **3a–b** (**2a** and **3a**: L^a= = $C_7H_4NS_2$; **2b** and **3b**: L^b = C_5H_4NS). In this article, we report how the incorporation of osmium influences the cooperative activation of boranes.

Results and discussion

Recently, we have synthesized the *cis* and *trans* isomers of Ru $[(PPh_3)_2(\kappa^2\text{-}N,S\text{-}C_7H_4NS_2)_2]$[19d] from the reaction of $[Ru(PPh_3)_3Cl_2]$ with a potassium salt of 2-mercaptobenzothiazole. With a similar objective, we performed the thermolysis of $[Os(PPh_3)_3Cl_2]$, **1**, with five equivalents of a potassium salt of two different heterocyclic systems L^a and L^b (L^a= = $C_7H_4NS_2$; L^b = C_5H_4NS). The salt elimination reactions afforded $[Os(PPh_3)_2(\kappa^2\text{-}N,S\text{-}C_7H_4NS_2)_2]$, **2a** (yield = 42%), and $[Os(PPh_3)_2(\kappa^2\text{-}N,S\text{-}C_5H_4NS)_2]$, **2b** (yield = 46%), respectively (Scheme 1). These

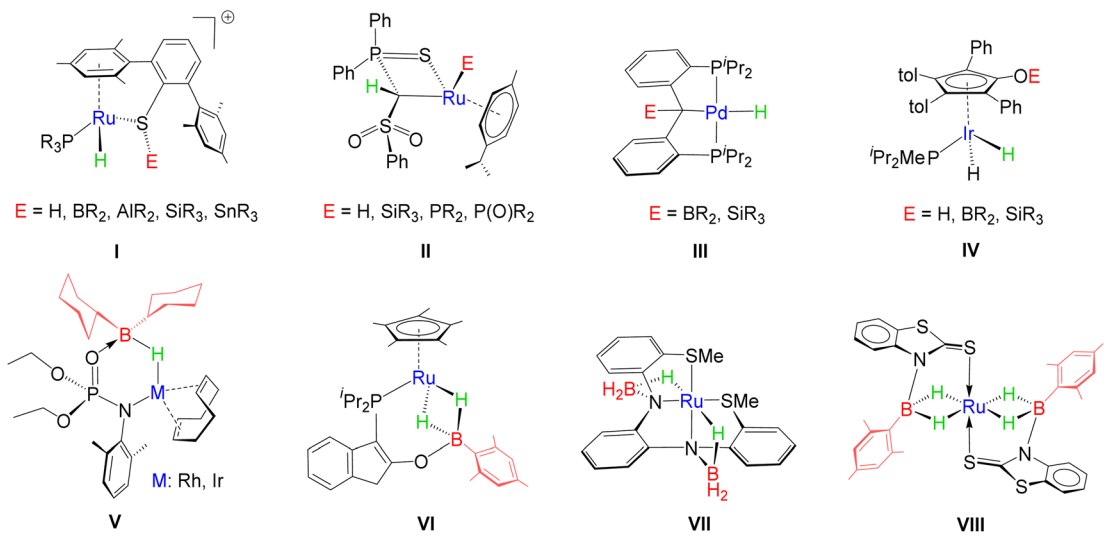

Chart 1 Various examples of small molecule activation by TM complexes (I–VIII). (^{i}Pr = isopropyl; R = =H, alkyl, aryl or alkoxy group).

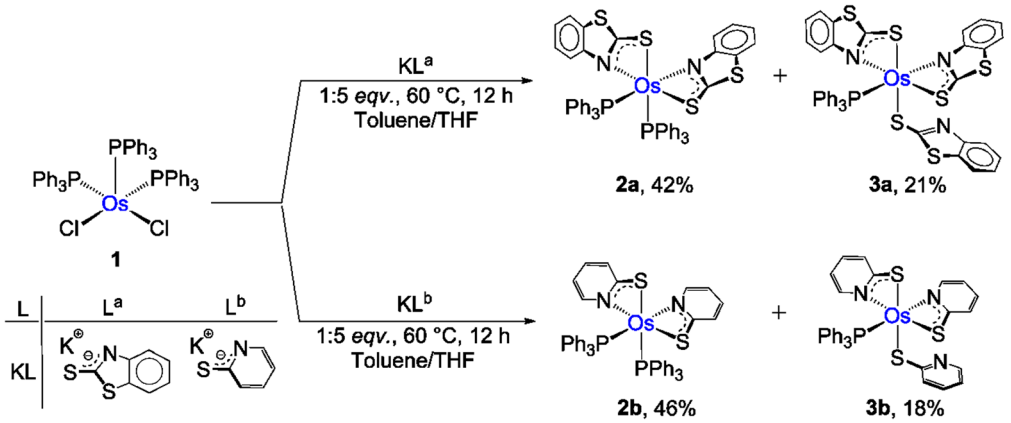

Scheme 1 Syntheses of Os(II) and Os(III)-*N*,*S*-chelated complexes.

complexes were isolated in their purest form by a chromatographic technique and were characterized by multinuclear spectroscopy, mass spectrometry and X-ray diffraction studies. Both species revealed single resonance peaks at $\delta = -5.5$ (**2a**) and −4.3 (**2b**) ppm in $^{31}P\{^1H\}$ NMR, respectively, indicating the presence of a single phosphorus environment. Along with the typical peaks related to the phenyl rings of PPh_3, the ^1H NMR spectrum showed additional aromatic region peaks in the range of $\delta = 6.12–7.95$ ppm that correspond to heterocyclic ring systems. To get a clear picture, X-ray diffraction analysis was performed on a suitable orange crystal of **2b**. As anticipated, the solid state X-ray structure of **2b** revealed an octahedral geometry around the Os center, featuring two κ^2-1,3-*N*,*S*-chelated rings and two triphenylphosphine ligands (Fig. 1). Taking into account that PPh_3 units are *cis* to each other, complex **2b** can be designated as *cis*-$[Os(PPh_3)_2(\kappa^2\text{-}N,S\text{-}C_5H_4NS)_2]$. The molecular ion peak in ESI-MS was in good agreement with the molecular formula. Moreover, in the case of **2a**, the intense ion peak at *m*/*z* 1049.1018 in mass spectrometry. This data in combination with spectroscopic analysis clearly supported the formation of analogous κ^2-1,3-*N*,*S*-chelated species, $[Os(PPh_3)_2(\kappa^2\text{-}N,S\text{-}L^a)_2]$.

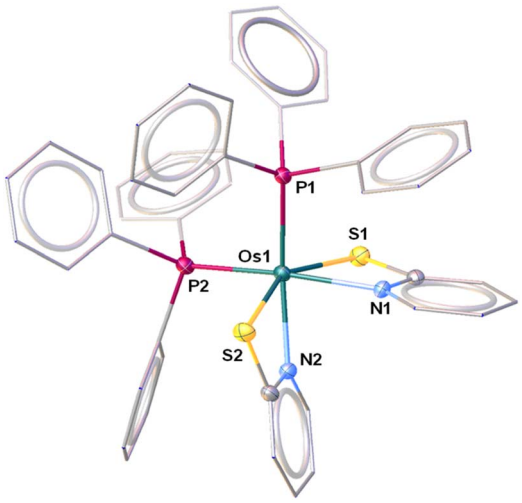

Fig. 1 Molecular structure and labelling diagram of **2b**. Selected bond lengths (Å) and bond angles (°) of **2b**: Os1–N1 2.143(3), Os1–N2 2.134(3), Os1–P1 2.2887(10), Os1–P2 2.2993(10), Os1–S1 2.4318(10), Os1–S2 2.4257(10); S2–Os1–S1 150.98(4), and N2–Os1–N1 80.11(13).

In parallel to the formation of **2a** and **2b**, the reactions also yielded **3a** (yield = 21%) and **3b** (yield = 18%), as green and violet solids, respectively. The molecular ion peaks in the ESI-MS spectra of **3a** and **3b** suggested that these species are analogous to each other with the generalised molecular formula $[Os(PPh_3)(L)_3]$ (**3a**: L = L^a; **3b**: L = L^b) (Fig. S10 and S12†). Neither the ^1H NMR nor the $^{31}P\{^1H\}$ NMR spectrum showed any prominent resonances that indirectly indicated their paramagnetic behaviour. Note that, recently, we have isolated paramagnetic Ru(III) species $[Ru(PPh_3)_2(\kappa^2\text{-}N,S\text{-}C_7H_4NS_2)_2(\kappa^1\text{-}S\text{-}C_7H_4NS_2)]$ by the aerial oxidation of a Ru(II)–borate complex.[19b] Similarly, **3a** and **3b** can be identified as the analogous paramagnetic complexes of Os(III) $[Os(Ph_3P)_2(\kappa^2\text{-}N,S\text{-}L)_2(\kappa^1\text{-}S\text{-}L)]$ (L = L^a or L^b), on the basis of mass spectrometry and preliminary spectroscopic data. Subsequently, the paramagnetic species **3a** and **3b** were investigated by electron paramagnetic resonance (EPR) spectroscopy and X-ray photoelectron spectroscopy (XPS).

Although the room temperature EPR spectra of both species in dichloromethane solution were ambiguous, the X-band frozen glass EPR spectra (Fig. S14†) displayed signals with *g* values of 2.157 (**3a**) and 2.136 (**3b**). Each spectrum exhibits rhombic features with no hyperfine coupling, presumably due to resolved ^{14}N and ^{31}P nuclei. Similar to analogous Ru species,[19b] *g* values differ significantly from those of organic radicals; thus, complexes can be described as a superposition of two resonating forms, *i.e.*, $[(L^-)Os^{III}]$ and $[(L^\bullet)Os^{II}]$. However, the majority of non-innocent ligand coordinated osmium complexes manifested a significant amount of ligand-based spin.[21] Conversely, the Mulliken spin density for the unpaired electron in **3a** and **3b** was located mostly on the Os atom (**3a**: +0.67; **3b**: +0.71) with a smaller contribution from the monodentate heterocyclic ligand (**3a**: +0.25; **3b**: +0.24), which was consistent with the spin density plot {Fig. 2(a) and (b)}. The molecular orbital analysis also showed that the unpaired electron typically accumulated on the orbital with a significant osmium d-character and a smaller p-character of the sulphur atom of the κ^1-*S* as well as the κ^2-*N*,*S*-ligand. Therefore, this

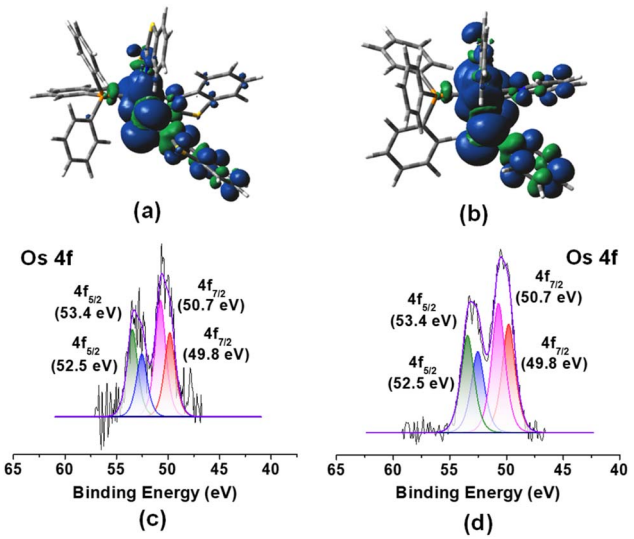

Fig. 2 Spin density plot for **3a** (a) and **3b** (b) (isovalue 0.004 [e $bohr^{-3}]^{1/2}$); X-ray photoelectron spectroscopy (XPS) spectra of Os $4f_{7/2}$ and $4f_{5/2}$ for **3a** (c) and **3b** (d).

result provides evidence of a predominantly metal-centred spin with a distinct contribution from the [$(L^{-})Os^{III}$] tautomer. Further, we have used X-ray photoelectron spectroscopy (XPS) to probe the presence of two tautomeric species in **3a–b**. Different sets of binding energies of Os $4f_{7/2}$ were observed in both species. The binding energy of 50.7 eV is associated with the [(L^{-})Os(III)] tautomer, while the relatively smaller value of 49.8 eV corresponds to the [$(L^{\bullet})$Os(II)]tautomer {Fig. 2(c) and (d)}. Extensive analysis of the XPS data indicated a greater contribution from the [(L^{-})Os(III)] tautomer as compared to [$(L^{\bullet})$Os(II)] species. These binding energy values closely resemble those of reported Os(III) and Os(II) species, respectively.[22] The characteristic elemental spectra of C, N, S, and P for both complexes were also investigated in a detailed analysis (Fig. S11 and S13†).

An important distinction between these two types of bis-κ^2-1,3-*N*,*S*-chelated complexes was the presence of a non-chelated κ^1-*S*-L ligand, thereby allowing us to compare the redox and photophysical properties explicitly. To investigate the redox activity of these complexes, we have recorded the cyclic voltammograms of **2a–b** in CH_2Cl_2 and **3a–3b** in CH_3CN {Fig. 3(a) and (b)}. The redox potential data referenced to the Fc^{+}/Fc couple are summarized in Table S1.† The cyclic voltammogram of **2a** yielded two quasi-reversible redox waves at $E_{1/2} = 0.191$ V and 0.948 V, while the same appeared at $E_{1/2} = -0.287$ V and 0.763 V for **2b**. In contrast, three quasi-reversible redox events were observed for **3a** in the potential window of 0 V to 1.0 V (Table S1†). The noteworthy observation is that a cathodic quasi-reversible wave at $E_{1/2} = -1.007$ V and −1.126 V was recorded for **3a** and **3b**, respectively.

Similar kinds of observations and assignments have been investigated for TM complexes containing N, S and P donor ligands. For example, Daly and co-workers demonstrated the redox events of a Ru complex comprising a triaryl non-innocent N_2S_2 ligand derived from *o*-phenylenediamine.[17b] Two reversible redox waves at −0.78 V and −0.28 V correspond to Ru^{II}/Ru^{I} and Ru^{III}/Ru^{II} redox couples, respectively, whereas the irreversible feature at −2.46 V appeared due to reduction of the *o*-diiminosemiquinone radical. Similarly, Heyduk illustrated that HAT (Hydrogen Atom Transfer) in the non-innocent tridentate [SNS] pincer based square planar nickel complex revealed one irreversible reduction at −2.74 V in addition to a reversible redox event at −0.64 V.[23] Mascharak and co-workers reported the cyclic voltammogram of [*cis*-(dppQ)$RuCl_2$] (dppQ = 1,2-bis-*N*-[2′ (diphenyl phosphanyl) benzoyl] benzoquinonediimine), wherein a dual ligand centered redox event was observed.[24] The ligand-centred reduction of the *o*-diiminosemiquinone radical to a fully reduced *o*-phenylenediamine unit was identified as the irreversible wave at −1.35 V, while the reversible wave at −0.28 V was assigned to the second ligand-centred redox event. Nevertheless, the Ru^{III}/Ru^{II} redox couple was attributed to the reversible wave at 0.90 V. In this context, [$Ru(Ph_3P)_2(\kappa^2$-*N*,*S*-$C_7H_4NS_2)_2(\kappa^1$-*S*-$C_7H_4NS_2)$], recently reported by us, revealed a reversible wave at 0.25 V associated with the $Ru^{II}(L^{\bullet})/Ru^{II}(L^{-})$ redox couple.[19b] Hence, the transition metal complexes derived from non-innocent ligands are known to exhibit rich redox chemistry.[25]

On the basis of these results, we have tentatively assigned the quasi-reversible feature of **2a** at 0.191 V and 0.948 V to the Os^{III}/

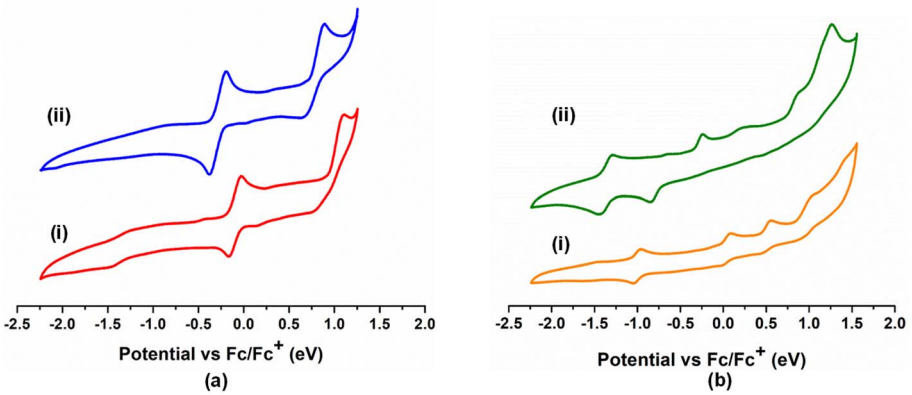

Fig. 3 (a) Cyclic voltammograms of **2a** (i) and **2b** (ii); (b) cyclic voltammograms of **3a** (i) and **3b** (ii).

Os^{II} and Os^{IV}/Os^{III} redox couples,[23] respectively. A similar trend was also observed for analogous **2b** in a slightly deviated electrochemical window, presumably due to the variation in the heterocyclic moiety. Notably, the cathodic quasi-reversible redox waves at −1.007 V (**3a**) and −1.126 V (**3b**) correspond to monodentate heterocyclic ligand (L^a and L^b) centred redox events, *i.e.*, the $Os^{II}(L^{\bullet})/Os^{II}(L^{-})$ couple.[23] Additionally, the cyclic voltammograms of **3a** and **3b** unveiled three sets of quasi-reversible redox waves, which were assigned to Os^{III}/Os^{II}, Os^{IV}/Os^{III} and Os^{IV}/Os^{V} redox couples, respectively (Table S1†).[23] Thus, it demonstrates the potential of these heterocyclic ligand systems (L^a and L^b) that can adopt a delocalised state of $[(L^{-})Os^{III}]$ and $[(L^{\bullet})Os^{II}]$ tautomers upon complexation and display a redox non-innocent nature.

In order to elucidate the photophysical properties associated with these κ^2-*N*,*S* chelated complexes, the UV-vis absorption spectra of **2a–b** and **3a–b** were recorded in CH_2Cl_2. All these species revealed strong absorption in the higher energy region due to the π–π* transition in aromatic rings. Some of the weak absorption peaks were additionally recorded in the window of 300–450 nm, which possibly occurred due to the charge transfer transition (MLCT). Slightly red shifted bands were observed in the case of mercaptobenzothiazolyl congeners. Intriguingly, the absorption features of **2a–b** and **3a–b** were approximately similar, except for the lower energy region, as illustrated in Fig. 4. The absorption spectrum of **3a** displayed a broad band at 650 nm, while the same band of **3b** appeared at 580 nm. The origin of these bands was interpreted by TD-DFT calculations in CH_2Cl_2. The calculated transitions at 666 nm for **3a** and 614 nm for **3b** correspond to an excitation from β-HOMO-2 to β-LUMO. Thus, the low energy transition can be presumably explained by the contribution of the $(L^{\bullet})Os^{II}$ radical, in which the non-chelated radical based ligands get reduced to their anionic form $[(L^{\bullet})Os^{II} \leftrightarrow (L^{-})Os^{III}]$. A similar phenomenon was also observed in the κ^2-*N*,*S* chelated Ru(III) species as well as amido ligand based Ru(III) species.[25a]

As a part of our ongoing research, we have developed polydentate ligand (N, S) based Ru(II) and Mo(II) complexes, which promoted B–H bond activation of free and bulky boranes.[19,20]

Based on MLC and hemilability present in κ^2-*N*,*S*-chelated metallacycles, the M–N bonds exhibit a tendency to capture boranes. Based on our previous studies, we have treated a stoichiometric amount of $BH_3 \cdot SMe_2$ with **2a** and **2b**, which led to the formation of **4a** and **4b**, respectively (Scheme 2). The ESI-MS spectrum of **4a** showed isotopic distribution patterns at *m*/*z* 1061.1318, which is consistent with the molecular formula [**2a** + BH_2]. The $^{31}P\{^1H\}$ NMR spectrum disclosed a singlet at δ = 19.2 ppm, which was shifted downfield in comparison to that of **2a**. The appearance of a new chemical shift at $\delta = -3.3$ ppm in the $^{11}B\{^1H\}$ NMR spectrum was attributed to the presence of a single boron environment. In addition to the presence of mercaptobenzothiazolyl and phenyl signals, the room temperature ^1H NMR spectra of **4a** unveiled two inequivalent hydridic signals at $\delta = -7.87$ and −13.26 ppm. Strikingly, the resonance at $\delta = -7.87$ ppm is broad in nature, while a more shielded signal at $\delta = -13.26$ ppm appeared as an apparent triplet ($^2J_{HP}$ = 18.5 Hz). Eventually, the former peak at $\delta = -7.87$ ppm corroborated the interaction of the metal with the B–H entity, resulting in an M–H–B motif. On the other hand, the higher-field signal at $\delta = -13.26$ ppm indirectly confirmed the presence of a metal hydride, which is *cis*-oriented to the phosphine ligands. Likewise, in **4b**, two distinct types of upfield ^1H NMR resonances at $\delta = -9.36$ and −12.57 ppm were detected. The $^{11}B\{^1H\}$ NMR spectrum of **4b** also featured a single chemical shift at δ = 10.1 ppm, which was shifted relatively downfield compared to that of **4a**. Moreover, ESI-MS revealed an intense ion peak at *m*/*z* 936.1506, which was associated with the formulation of $C_{46}H_{38}N_2S_2P_2Os$. Systematic investigation by NMR spectroscopy along with mass spectrometry clearly suggests that compound **4b** is analogous to **4a** (see the ESI†). Finally, in order to confirm the spectroscopic assignments, a single-crystal X-ray diffraction study was performed on one of the complexes.

The X-ray diffraction study of **4a** was carried out on an orange crystal obtained from hexane layered CH_2Cl_2 solution. The geometry around the osmium center can be viewed as a distorted octahedral geometry with a void at the axial position. As shown in Fig. 5, the osmium center in the particular octahedral geometry is supported by two homoleptic sulphur atoms of the mercaptobenzothiazolyl entity, two phosphorus atoms of the PPh_3 ligand and a bridging hydride of the BH_2 moiety. Although, Os–H was not detected in the solid state X-ray

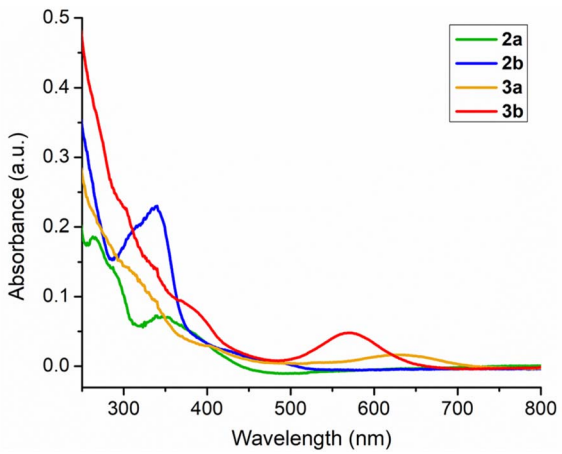

Fig. 4 Combined UV-vis spectra of **2a**, **2b**, **3a** and **3b**.

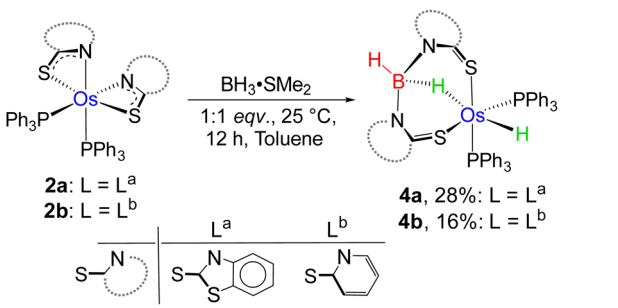

Scheme 2 B–H activation by Os(II)–*N*,*S*-chelated complexes, **2a–b**.

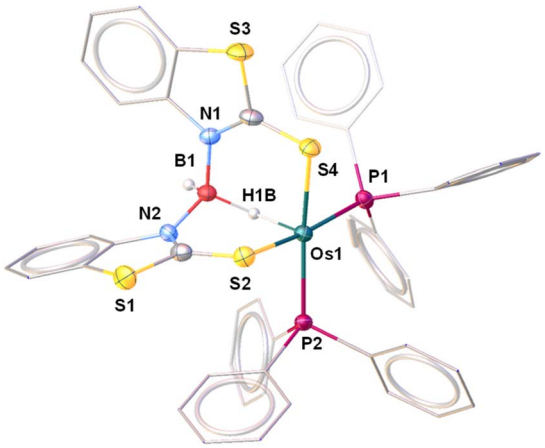

Fig. 5 Molecular structure and labelling diagram of **4a**. Selected bond lengths (Å) and bond angles (°) of **4a**: Os1–P2 2.3048(10), Os1–P1 2.3085(11), Os1–S4 2.3675(10), Os1–S2 2.3985(11), Os1–B1 2.689; P2–Os1–P1 97.83(4), and P2–Os1–S4 170.54(4).

diffraction analysis, we believe that a hydrogen atom occupies the vacant site of the octahedron. The presence of Os–H can also be elucidated by the aforementioned sharp hydridic resonance signal at $\delta = -13.26$ ppm in the ^{1}H NMR spectrum, which remained unperturbed on decoupling to ^{11}B (Fig. S18†). The Os1–B1 separation of 2.689 Å is significantly longer than that of various osmium boryl species,[26] but still in good agreement with that of reported σ-borate species[27,28] of ruthenium.[29] Therefore, this can be better emphasized as a δ(B–H) agostic interaction, having primary σ(B–H) as well as secondary interactions through sulphur with metal.[27a] Indeed, the species **4a** and **4b** were well identified as the Os(σ-borate)hydride complex, $[Os(PPh_3)_2(H)\{\kappa^3\text{-}H,S,S'\text{-}H_2B(L^a/L^b)_2\}]$. Based on previous reports,[3b,c,15,16] we believe that the formation of Os(σ-borate) hydride species, **4a–b**, presumably occurred *via* a few concerted steps: (i) cleavage of one hemilabile Os–N bond and cooperative B–H bond activation that eventually formed an Os(II) hydride, (ii) cleavage of another hemilabile Os–N bond and formation of a B–N bond, and (iii) activation of another B–H bond of the BH_2L_2 unit to form Os(σ-borate) species. Considering this fact, the event can be rationalized as the activation of two B–H bonds in borane.

Density functional theory (DFT) studies aided us to gain insight into the energetics as well as to differentiate the bonding and electronic properties between **4a** and **4b**. The changes in the Gibbs free energy (ΔG) of these reactions **3a–b** → **4a–b** were highly negative, implying the thermodynamic spontaneity of the borane activation reaction. Interestingly, the more negative value of ΔG for **3a** → **4a** showed the more feasibility of borane activation in the case of the mercaptobenzo-thiazolyl analogue. Further, the second-order perturbation theory suggested a donor–acceptor interaction between σ(B–H) and Os in **4a–b**, but a lower stabilization energy was observed for **4a**. Natural bonding orbital (NBO) analysis of **4b** revealed that the electron population of the B–$H_{bridging}$ bonding orbital in both species is lower than that of the non-bonding B–H orbital in free borane, clearly indicating the formation of a σ-borate unit through B–H activation. The electron population and Wiberg bond indices (WBI) of the B–$H_{bridging}$ bonding orbital possess relatively smaller values for **4b** in comparison to **4a**. This implied an uneven σ-donation from σ(B–H) to the metal center, which presumably occurred due to the presence of different heterocyclic counterparts. As shown in Fig. 6(b), significant bonding interactions along Os–H bonds were also observed in these species, which is consistent with their high WBI values. Furthermore, topological analyses of the electron densities of **4a** and **4b** were performed using the quantum theory of atoms in molecules (QTAIM). The contour line diagram showed bond critical points (BCPs) between Os–H and B–H bonds in the Os–H–B plane. However, no BCP was located between osmium and boron, which indicated the absence of any strong bonding interaction.

Esteruelas and co-workers[30] have extensively studied the structure and bonding of distinct types of osmium σ-borane species, which allowed us to perform a comparative study of **4a–b** based on their structural parameters and spectroscopic data (Table 1). The very first structurally characterized bis-σ-borane complex of osmium, $[Os(H)_2(\eta^2\text{:}\eta^2\text{-}H_2BCH_2Ph)(^iPr)(P^iPr_3)]$,[30a] **IX**, was obtained by the successive hydrogenation and hydroboration of a cationic Os–alkylidene complex, [OsH(OH)(≡CPh)(IPr)(P^iPr_3)] [OTf]. The same group also reported a novel σ(B–H) complex of osmium, $[OsH(\eta^3\text{-}H_2BCat)(\eta^2\text{-}HBCat)(P^iPr_3)_2]$[30b], **X**, offering η^2-coordinated elongated σ-borane and η^3-coordinated bis(elongated σ)-dihydridoborate entities. Moreover, the σ(B–H)-borinium derivative,[30c] **XI**, exhibited a downfield ^{11}B NMR chemical shift, certainly emerged due to high cationic charge density on borinium boron. Consequently, the Os–B bond length is notably shorter in the η^2-BH coordination entity of **XI**. Further, based on spectroscopic, structural and theoretical

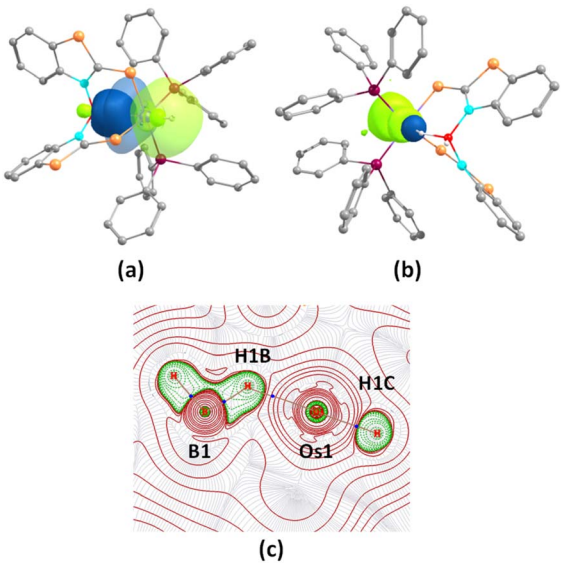

Fig. 6 (a) Donor–acceptor interaction between σ(B–H) and the Os center in **4a**; (b) Os–H bonding interaction in **4a** (isovalue 0.004 [*e* bohr^{-3}]$^{1/2}$); (c) contour-line diagram of the Laplacian of the electron density along Os–H–B planes in **4a**.

Table 1 Selected structural parameters and NMR chemical shifts of some osmium σ-borane/borate complexes[a]

Os-(σ-borane/borate)	Spectroscopic parameter		
	^{1}H NMR[b]	^{11}B NMR[b]	$d_{av.M-B}$ (Å)
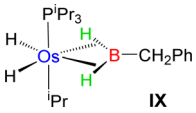 IX	−8.26 −9.40	81.0	1.913(4)
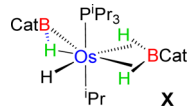 X	−9.50	35.0	2.112(4) 2.159(4)
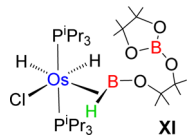 XI	−4.0 −6.9 −16.3	55.0	1.899(7)
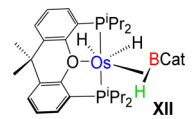 XII	−1.53 −5.60 −18.80	45.5	2.057(4)
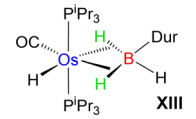 XIII	−5.67 −7.07	21.0	2.331(3)
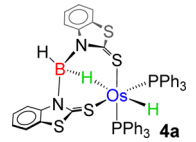 4a	−7.87 −13.26	−3.3	2.689
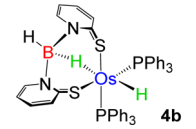 4b	−9.36 −12.57	10.1	—

[a] ^{i}Pr = isopropyl; Cat = catechol. [b] in ppm.

points of view, Esteruelas described a novel osmium POP-pincer skeleton stabilized σ-borane complex,[30d] **XII**, bearing two hydrides and a σ(B–H) moiety. It is worth noting that the ^{11}B NMR resonance associated with Os(σ-borate) complexes, **4a–b**, appeared significantly upfield shifted in comparison to the aforementioned osmium σ-borane complexes (**IX–XII**). The observation can be well explained on the basis of reduced bonding interaction between the metal and boron in **4a–b**, which is also reflected in the longer M–B separation. Apart from a variety of σ-borane complexes of osmium, Braunschweig reported tris-isopropyl based Os dihydridoborate species,[31] **XII**. It also shows inequivalent characteristic structural and spectroscopic properties in respect of **4a–b**. This fascinating mode of bonding can be described on the basis of the anionic borate nature of the $BH_2(L^a/L^b)_2$ counterpart, which eventually restricted the π-backdonation from the metal to the ligand.[27a] For this reason, species **4a–b** can be considered as one of the newest and most unique additions in the series of osmium σ-complexes.

We have observed that complexes, **2a–b**, readily undergo a borane activation reaction by ring opening of two hemilabile four-membered OsNCS cycles. Similarly, the paramagnetic species **3a–b** are composed of two osma-heterocyclic entities. However, the salient difference between the two types of complexes can be rationalized by the presence of the non-innocent ligand. Transition metal complexes with redox non-innocent ligands in combination with MLC activate BH_3 and 9-BBN molecules.[8c,32] The isolation of **VIII** (*vide supra*, Chart 1) by the B–H activation of the abovementioned κ^2-*N*,*S*-chelated ruthenium complex, $[Ru(Ph_3P)_2(\kappa^2\text{-}N,S\text{-}C_7H_4NS_2)_2(\kappa^1\text{-}S\text{-}C_7H_4NS_2)]$, is one of the prominent examples in this perspective.[19b] These results encouraged us to investigate the combined effect of non-innocent ligands and heavier transition metals in the B–H bond activation process. Thus, we have explored the reactivity of **3a** and **3b** with smaller boranes employing different reaction conditions (Scheme 3).

The stoichiometric addition of $BH_3{\cdot}SMe_2$ into a solution of **3b** at room temperature showed a gradual colour change from violet to yellow and yielded **5** in 18% yield along with some air and moisture sensitive products. The complex was further purified using thin layer chromatography and was characterised using different spectroscopic techniques. Unlike **4a–b**, the high-field region in the ^{1}H NMR spectrum of **5** disclosed two broad resonances at $\delta = -13.65$ and -13.67 ppm, which indicated the presence of two non-equivalent Os–H–B protons. Interestingly, the resonance signal in the $^{11}B\{^{1}H\}$ NMR spectrum appeared relatively downfield shifted at $\delta = 62.5$ ppm. The retention of a single phosphine unit was predicted from the peak at $\delta = 16.4$ ppm in $^{31}P\{^{1}H\}$ NMR. Moreover, the ESI-MS spectrum of **5** showed a molecular ion peak at *m*/*z* 703.0827 with isotopic distribution patterns. However, a clear account could not be envisaged until the single-crystal X-ray diffraction analysis of **5** was carried out.

The molecular structure of **5** can be designated as the κ^2-*N*,*S*-chelated osmium(II) dihydridoborate complex, $[Os(PPh_3)(\kappa^2\text{-}N,S\text{-}C_5H_4NS)\{\kappa^3\text{-}H,S,S'\text{-}H_2B(OH)(C_5H_4NS)\}]$ (Fig. 7). The formation of the Os(dihydridoborate) unit clearly suggests the

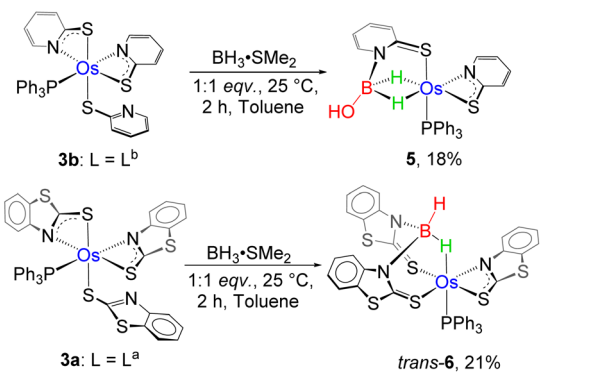

Scheme 3 B–H activation by paramagnetic Os(III)-*N*,*S*-chelated species, **3a–b**.

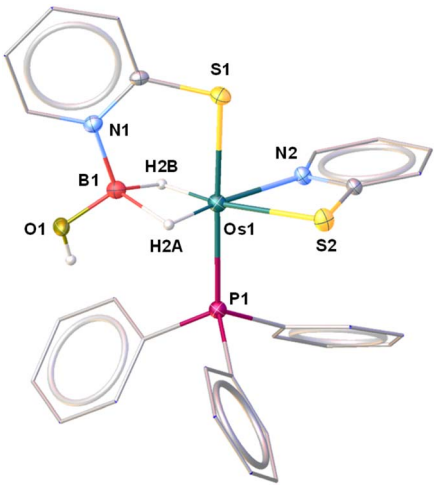

Fig. 7 Molecular structure and labelling diagram of **5**. Selected bond lengths (Å) and bond angles (°) of **5**: Os1–S1 2.3669(9), Os1–S2 2.5045(9), Os1–B1 2.059(4), B1–O1 1.371(5), and B1–Os1–N2 145.20(13).

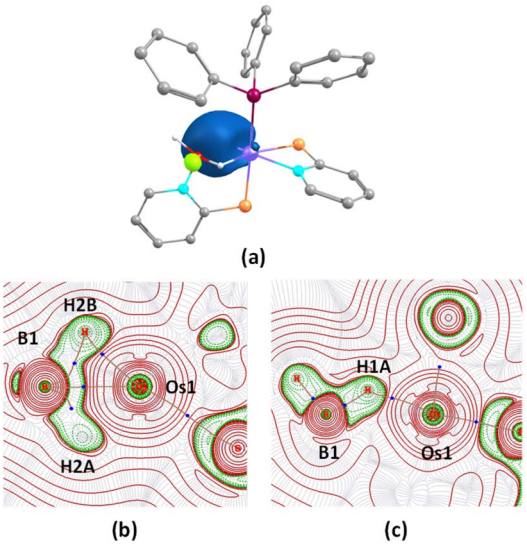

Fig. 8 (a) 3c-2e bonding interaction along the Os–H–B plane in **5′** (isovalue 0.004 [e bohr^{-3}]$^{1/2}$); (b and c) contour-line diagram of the Laplacian of the electron density along the Os–H–B planes in **5′** and *trans*-**6**, respectively.

insertion of borane across the Os–N bond of one of the hemilabile OsNCS metallacycles, followed by the removal of the κ^1-*S*-C_5H_4NS ligand. However, we believe that the addition of $BH_3\cdot SMe_2$ into a solution of **3b** initially led to the formation of a H-substituted Os–dihydridoborate complex, [Os(PPh_3)(κ^2-*N*,*S*-C_5H_4NS){κ^3-*H*,*H*,*S*-$H_3B(C_5H_4NS)$}], **5′**, which further gets converted to **5** upon hydrolysis by a trace amount of water during chromatographic separation. It was further established by the deshielded chemical shift at δ = 3.81 ppm in ^{1}H NMR and significantly low-field $^{11}B\{^1H\}$ NMR resonance. In this context, Stradiotto isolated a Ru–dihydridoborate complex, [Cp*Ru(κ^3-*P*,*H*,*H*-(^{i}Pr))P-($C_9H_6OH_2B$-Mes)], by the activation of BH_2Mes (*vide supra*, **VI**, Chart 1).[16] Also, a piano-stool Fe–dihydridoborate complex[5c] was reported by Liang *et al.* and was generated by cooperative B–H bond activation utilizing [(Cp*L″Fe)(μ-N_2)(FeCp*L″)] (L″ = deprotonated *N*-picoly N-heterocyclic carbene ligand). The Os–B separation of 2.057 Å in **5** is in good agreement with the M–B bond lengths of the abovementioned lighter congener dihydridoborate species.[29] Moreover, the same parameter is marginally shorter in comparison to the Ru–B distances of Ru–σ-borane(dihydridoborate) species [Ru(PCy_3)$_2${Bpin(μ-H)$_2$}(H){(μ-H)Bpin}] (2.188(5) Å),[33] reported by Sabo-Eteinne, and Ru-bis(dihydridoborate) species, [Ru{(μ-H)$_2$BH(C_5H_4NS)}$_2$] (2.161(8) Å),[29b] reported by our group.

To get insight into the bonding situations in dihydridoborate coordination, we have carried out DFT calculations on model system **5′**. The four-membered cyclic **5′** possessed a BCP along the Os–B bond in addition to two other BCPs along B–H and one Os–H bonds, respectively. In this particular topology, the bond paths were inwardly curved {Fig. 8(b)}, which strongly resembles the situation of diborane (**6**). The BCPs associated with Os–H and B–H bond paths have significantly large ellipticity, ∈, and considerably smaller negative energy density, H(*r*) values, thus reflecting the presence of an anisotropic σ(B–H) agostic interaction with metal. In this context, a strong 3c–2e bonding interaction along Os–H–B was observed in the Os–dihydridoborate complex, **5′** {Fig. 8(a)}, in NBO calculation. The computed natural charge on the boron atom further well agreed with a greater charge accumulation in the case of **5′** than that of **4a–b**. It clearly addressed the manifestation of a stronger Os–B bonding interaction in the dihydridoborate component than the σ-borate moiety.

On the other hand, the reaction of **3a** with $BH_3\cdot SMe_2$ yielded compound **6** as a red crystalline solid in 15% yield. The single peak at δ = 9.1 ppm in the $^{31}P\{^1H\}$ NMR spectrum of **6** suggested the retention of the phosphine unit of **3a**. The $^{11}B\{^1H\}$ NMR spectrum showed a sharp peak at δ = −3.7 ppm, which was observed considerably in the upfield region relative to **5**. Along with the signal corresponding to the aromatic hydrogens, a high-field broad resonance was also detected at δ = −4.56 ppm in the ^{1}H NMR spectrum of **6**, which probably emerged due to the presence of Os–H–B. In addition to Os–H–B, another broad signal at δ = 5.15 ppm in ^{1}H NMR resolved upon decoupling to boron, seemingly appeared due to the presence of terminal B–H. Furthermore, ESI-MS exhibited a molecular-ion peak at *m*/*z* 965.0099 with an isotopic distribution pattern, which is consistent with the molecular formula $C_{39}H_{29}N_3S_6$-OsPB. Although the spectroscopic assessment proposed the probable activation of the B–H bond, a precise explanation could not be envisaged until the single-crystal X-ray diffraction investigation was performed.

As shown in Fig. 9(left), the molecular structure of **6** can be identified as a κ^2-*N*,*S*-chelated osmium(II) mercaptobenzo–thiazolyl borate complex. Similar to **4a**, the distorted octahedral geometry around the Os center in **6** is composed of $[H_2BL_2]^-$ in κ^3-(*H*,*S*,*S′*) coordination mode, featuring comparable separation between metal and boron. Although we were unable to find any proper mechanistic evidence behind the formation of **6**, we assumed that the reaction progressed *via* two steps. The first

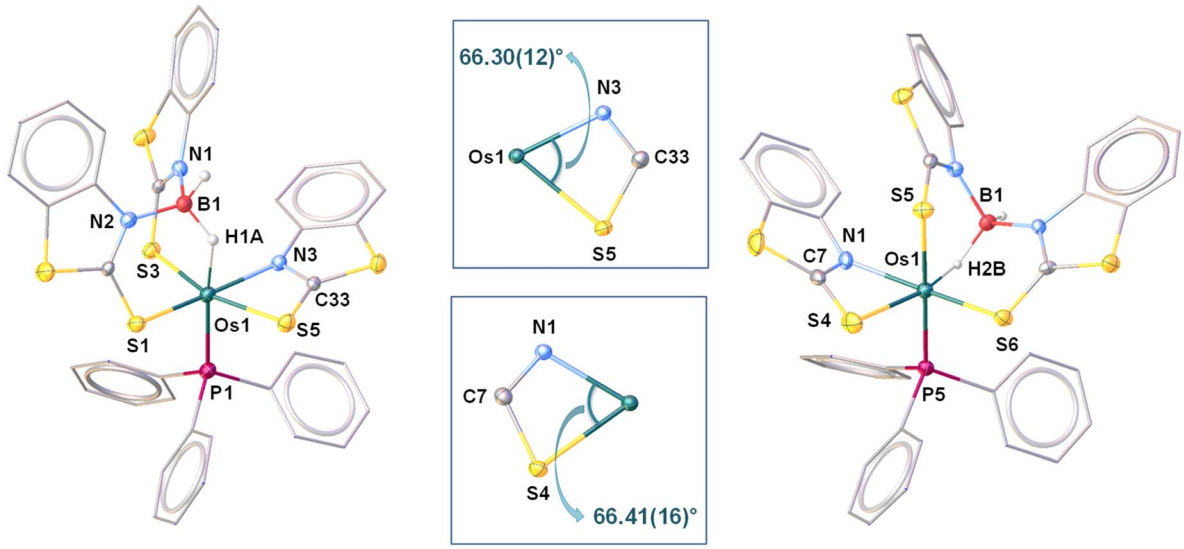

Fig. 9 Molecular structure and labelling diagram of *trans*-**6** (left) and *cis*-**6** (right). Selected bond lengths (Å) and bond angles (°) of *trans*-**6**: Os1–B1 2.712, Os1–N3 2.127(4), Os1–S5 2.4816(15), and Os1–S1 2.3162(15); N3–Os1–S5 66.30(12). Selected bond lengths (Å) and bond angles (°) of *cis*-**6**: Os1–B1 2.497(8), Os1–N1 2.138(5), Os1–S4 2.4741(18), and Os1–S5 2.4852(17); N1–Os1–S4 66.41(16).

step involved the capture of the BH_2 bond after two Os–N bond cleavages, which resulted in a σ-borate counterpart. Then, the chelation of the κ^1-*S*-L^a ligand through Os–N bond formation led to the generation of an osma-heterocycle (OsNCS) in the second step. Based on the *trans* orientation of the hydride ligand with respect to phosphine, we have designated the species as *trans*-**6**. Moreover, tris-homoleptic mercaptobenzothiazolyl sulphur moieties were coordinated to the osmium center in a meridional fashion. Thus, **6** can be well described as *trans-mer*-[Os$(PPh_3)(\kappa^2$-*N*,*S*-$C_7H_4NS_2)\{\kappa^3$-*H*,*S*,*S*′-$H_2B(C_7H_4NS_2)_2\}$], which is analogous to [Ru$(PPh_3)(\kappa^2$-*N*,*S*-$C_7H_4NS_2)\{\kappa^3$-*H*,*S*,*S*′-$H_2B(C_7H_4NS_2)_2\}$],[19c] isolated from the reaction of $[(\eta^6$-*p*-cymene)$RuCl_2PPh_3]$ with $Na[H_2B(C_7H_4NS_2)_2]$. Further, QTAIM analysis revealed that bond critical points (BCPs) were detected along Os–H and B–H bonds in the Os–H–B plane of *trans*-**6** {Fig. 8(c)}. In contrast to **5**, relatively lower ellipticity, ∈ values are observed for Os–H and B–H bonds. Subsequently, NBO analysis also addressed the distinct type of bonding scenario in *trans*-**6**. Rather than the 3c–2e bonding interaction, Os(σ-borate) species displayed a donor–acceptor interaction, in which the filled σ(B–H) orbital donates electron density to an empty metal orbital.

The coordination chemistry of TM σ-borate complexes has become a significant research topic due to their ability to adopt versatile coordination geometries around metal centres. Recently, our group has carried out an explicit structural investigation on several stereoisomers of κ^2-*N*,*S*-chelated Ru(II) mercaptobenzothiazolyl borate complexes.[19d] The formation of *trans*-**6**, therefore, tempted us to investigate the efficient synthetic pathway for the synthesis of its *cis* analogue, *i.e. cis*-**6**. Thus, we have carried out the thermolysis of $[Os(PPh_3)_3Cl_2]$, **1**, with two equivalents of [bis-(2-mercapto-benzothiazolyl)borate], which led to the formation of *cis*-**6** along with **2a**, **3a** and *trans*-**6** (Scheme 4).

The solid-state structure revealed a distorted octahedral geometry, in which three sulphur atoms are present on one of the triangular faces {Fig. 9(right)}. Unlike *trans*-**6**, the bridging hydride was placed *cis* to the phosphine ligand. As a result, it can be described as *cis*-**6**, more specifically *cis-fac*-**6**. Both of the isomers exhibited comparable bite angle values for the four-membered chelating osmacycles, which suggested that the borate counterpart has no significant steric influence on the coordination of the bidentate mercaptobenzothiazolyl ligand. In this connection, the hydridic chemical shift of *cis*-**6** at $\delta = -13.83$ ppm related to Os–H–B appeared in the relatively upfield region in comparison to *trans*-**6**. The *trans*-isomer was composed of a good σ-donor phosphine ligand *trans* to the hydride, whereas the electronegative S atom occupied the *trans* site of the hydride in the *cis* isomer. The electron donation from

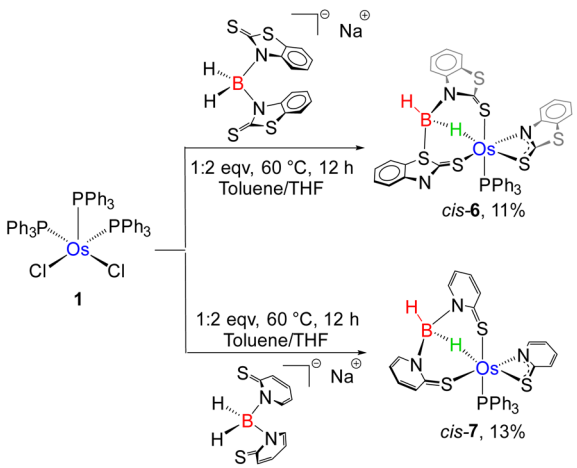

Scheme 4 Modified syntheses of isomeric Os(σ-borate) species, *cis*-**6** and *cis*-**7**.

the B–H bond to the metal centre is expected to be more, where sulphur is the *trans* atom. Therefore, the hydridic character of Os–H–B is greater in *cis*-**6** in comparison to *trans*-**6**. However, the $^{11}B\{^1H\}$ NMR resonance of both isomers remained unperturbed instead of adapting different spatial arrangements.

The effect of structural variation on the thermodynamic and kinetic stability of these isomeric species was analysed by means of DFT studies. The structural parameters of the optimized geometries agreed well with those obtained from the X-ray diffraction data. However, the Os–B separation in *cis*-**6** was slightly elongated compared to that found in the solid-state structure (Table S2†). The relative thermodynamic stability of *trans*-**6** can be described on the basis of ground-state energy calculations. The energy difference between these two isomers is 1.2 kcal mol^{-1}. On the other hand, molecular orbital (MO) analysis suggested that the HOMOs of both isomers were mainly localized on the d-orbitals of osmium centres with a weak π-bonding interaction along the C=S bond. Meanwhile, a delocalized electron density over the heterocyclic ring of the σ-borate unit was observed in LUMOs. The energy gap between the HOMO and LUMO, $\Delta E_{HOMO-LUMO}$, of *cis*-**6** is quite higher than that of *trans*-**6**, which presumably indicated the greater kinetic stability of the *cis*-isomer (Fig. 10). Therefore, *trans*-**6** is a thermodynamically controlled product, while the formation of *cis*-**6** is seemingly kinetically favoured.

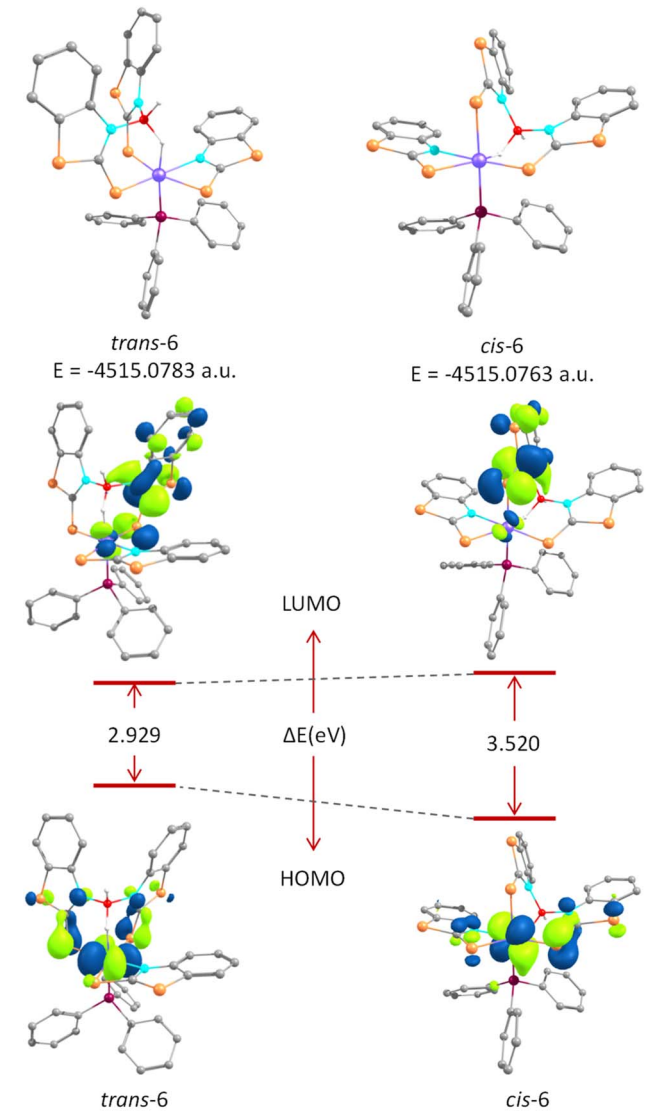

Fig. 10 Top: ground-state energies of *trans*-**6** (left) and *cis*-**6** (right). Bottom: HOMO–LUMO energy gap between *trans*-**6** and *cis*-**6**.

In stark contrast, we were unable to isolate the mercaptopyridinyl analogue of *trans*-**6** or *cis*-**6**, while the borane activation was carried out using $[Os(Ph_3P)(\kappa^2\text{-}N,S\text{-}C_5H_4NS)_2(\kappa^1\text{-}S\text{-}C_5H_4NS)]$, **3b**. Thus, we have imitated the methodology that was employed to synthesise *cis*-**6**, which is the treatment of **1** with 2 equivalents of $NaBH_2L^b{}_2$. Indeed, the reaction led to the formation of **7** along with the formation of **2b**, **3b**, **4b** and **5**. The ^1H NMR chemical shift related to Os–H–B of **7** ($\delta = -12.46$ ppm) was in the upfield region compared to that of analogous *trans*-**6** ($\delta = -4.60$ ppm), but closely resembles that of *cis*-**6** ($\delta = -13.81$ ppm). The single chemical shift at $\delta = 13.9$ ppm in the $^{11}B\{^1H\}$ NMR of **7** was associated with the tetra-coordinated boron atom. The boron centre in all these σ-borate complexes exhibited a diverse electronic nature, predominately due to the presence of different heterocyclic entities and various possible geometrical orientations. Indeed, the solid-state X-ray structure, shown in Fig. S1,† revealed that the hydrides of the σ(B–H) moiety and PPh_3 ligand were placed in the axial and equatorial positions of the octahedron, respectively. This confirmed that the geometry of **7** can be considered as a *cis* isomer. Moreover, three homoleptic sulphur atoms occupied three vertices of one of the triangular faces. Thus, the latter complex can be better designated as *cis-fac*-$[Os(PPh_3)(\kappa^2\text{-}N,S\text{-}C_5H_4NS)\{\kappa^3\text{-}H,S,S'\text{-}H_2B(C_5H_4NS)_2\}]$. The Os–B bond distance of 2.497 Å was in good accord with analogous *cis*-**6**, but evidently shorter than that of *trans*-**6**. The bite angle (N–Os–S) of the four membered metallacycle in *cis*-**7** is akin to those of the analogous isomeric species.

Conclusions

In summary, we have developed a series of osmium bis-κ^2-*N*,*S*-chelated complexes featuring hemilabile osma-heterocycles that illustrate their susceptibility towards activation of B–H bonds in free boranes. Subsequently, we have investigated the redox, photochemical and electronic behaviour to differentiate between various diamagnetic and paramagnetic bis-κ^2-*N*,*S*-chelated species. Cooperative activation of free boranes by diamagnetic complexes led to the formation of Os(σ-borate) hydride complexes through dual non-identical B–H bond activation. In contrast, two redox-active paramagnetic bis κ^2-*N*,*S*-chelated species possessing different non-innocent heterocyclic ligands unveiled different patterns of activation. The capture of the B–H bond by the cleavage of the Os–N bond in hemilabile osma-heterocycles yielded dihydridoborate and σ-borate complexes of osmium, respectively. To investigate the influence of spatial arrangements on the stability and bonding of isomeric species, we have further isolated several isomeric Os(σ-borate) complexes. In the course of our study, combined

experimental and theoretical studies show that a combination of electronic behaviour and metal–ligand cooperativity significantly influences the activation of borane.

Data availability

The data supporting this article have been included as part of the ESI.†

Author contributions

S. Gayen, F. Assanar, S. Shyamal and D. P. Dorairaj have executed the experimental synthesis, characterization and analysis of the data. S. Gayen has conducted the theoretical calculations. All authors have contributed to the preparation of the manuscript. S. Ghosh has supervised the project.

Conflicts of interest

There are no conflicts to declare.

Acknowledgements

We thankfully acknowledge the support from SERB-DST (Grant No. CRG/2023/000189), New Delhi, India. S. G. thanks CSIR, F. A and S. S. thank UGC, and D. P. D thanks IIT Madras for research fellowships. The computational facility of IIT Madras is gratefully acknowledged.

Notes and references

1 (*a*) R. Peters, *Cooperative Catalysis*, Wiley-VCH, Weinheim, 2015; (*b*) C. Gunanathan and D. Milstein, *Acc. Chem. Res.*, 2011, **44**, 588–602; (*c*) R. H. Morris, *Acc. Chem. Res.*, 2015, **48**, 1494–1502.

2 (*a*) M. R. Elsby and R. T. Baker, *Chem. Soc. Rev.*, 2020, **49**, 8933–8987; (*b*) H. Li, T. P. Goncalves, D. Lupp and K.-W. Huang, *ACS Catal.*, 2019, **9**, 1619–1629.

3 (*a*) T. Higashi, S. Kusumoto and K. Nozaki, *Chem. Rev.*, 2019, **119**, 10393–10402; (*b*) L. Omann, C. D. F. Konigs, H. F. T. Klare and M. Oestreich, *Acc. Chem. Res.*, 2017, **50**, 1258–1269; (*c*) K.-S. Feichtner and V. H. Gessner, *Chem. Commun.*, 2018, **54**, 6540–6553; (*d*) F. Forster and M. Oestreich, *Metal-Ligand Cooperative Si–H Bond Activation in Organosilicon Chemistry – Novel Approaches and Reactions*, ed. T. Hiyama, and M. Oestreich, Wiley-VCH, Weinheim, 2019, pp. 115–130.

4 (*a*) C. C. Comanescu and V. M. Iluc, *Chem. Commun.*, 2016, **52**, 9048–9051; (*b*) C. C. Comanescu and V. M. Iluc, *Polyhedron*, 2018, **143**, 176–183; (*c*) J. Y. Corey, *Chem. Rev.*, 2016, **116**, 11291–11435; (*d*) M. K. Bisai, V. Sharma, R. G. Gonnade and S. S. Sen, *Organometallics*, 2021, **40**(13), 2133–2138.

5 (*a*) J. B. Geri and N. K. Szymczak, *J. Am. Chem. Soc.*, 2015, **137**, 12808–12814; (*b*) C. Erken, A. Kaithal, S. Sen, T. Weyhermuller, M. Holscher, C. Werle and W. Leitner, *Nat. Commun.*, 2018, **9**, 4521; (*c*) Q. Liang, H. A. Garcia Mayerstein and D. Song, *Organometallics*, 2023, **42**, 816–824.

6 (*a*) S. P. Cronin, J. M. Strain, M. S. Mashuta, J. M. Spurgeon, R. M. Buchanan and C. A. Grapperhaus, *Inorg. Chem.*, 2020, **59**, 4835–4841; (*b*) R. Stichauer, A. Helmers, J. Bremer, M. Rohdenburg, A. Wark, E. Lork and M. Vogt, *Organometallics*, 2017, **36**, 839–848; (*c*) I. Heuermann, B. Heitmann, R. Stichauer, D. Duvinage and M. Vogt, *Organometallics*, 2019, **38**, 1787–1799; (*d*) R. Stichauer and M. Vogt, *Organometallics*, 2018, **37**, 3639–3643.

7 (*a*) J. W. Nugent, M. Garcia-Melchor and A. R. Fout, *Organometallics*, 2020, **39**, 2917–2927; (*b*) X. Zhai, M. Pang, L. Feng, J. Jia, C.-H. Tung and W. Wang, *Chem. Sci.*, 2021, **12**, 2885–2889; (*c*) J. V. Obligacion and P. J. Chirik, *ACS Catal.*, 2017, **7**, 4366–4371; (*d*) S.-F. Hou, J.-Y. Chen, M. Xue, M. Jia, X. Zhai, R.-Z. Liao, C.-H. Tung and W. Wang, *ACS Catal.*, 2020, **10**, 380–390.

8 (*a*) M. Ito, M. Itazaki and H. Nakazawa, *Inorg. Chem.*, 2017, **56**, 13709–13714; (*b*) J. B. Geri and N. K. Szymczak, *J. Am. Chem. Soc.*, 2015, **137**, 12808–12814; (*c*) H. Song, K. Ye, P. Geng, X. Han, R. Liao, C.-H. Tung and W. Wang, *ACS Catal.*, 2017, **7**, 7709–7717.

9 (*a*) S. R. Flynn and D. F. Wass, *ACS Catal.*, 2013, **3**, 2574–2581; (*b*) A. R. Jupp and D. W. Stephan, *Trends Chem.*, 2019, **1**(1), 35–48; (*c*) E. R. M. Habraken, A. R. Jupp, M. B. Brands, M. Nieger, A. W. Ehlers and J. C. Slootweg, *Eur. J. Inorg. Chem.*, 2019, 2436–2442; (*d*) J. Bauer, H. Braunschweig and R. D. Dewhurst, *Chem. Rev.*, 2012, **112**, 4329–4346.

10 B. Chatterjee, W.-C. Chang, S. Jena and C. Werle, *ACS Catal.*, 2020, **10**, 14024–14055.

11 (*a*) A. Lefranc, Z.-W. Qu, S. Grimme and M. Oestreich, *Chem.–Eur. J.*, 2016, **22**, 10009–10016; (*b*) T. Stahl, K. Mether, Y. Ohki, K. Tatsumi and M. Oestreich, *J. Am. Chem. Soc.*, 2013, **135**, 10978–10981; (*c*) F. Forster, T. T. Metsanen, E. Irran, P. Hrobarik and M. Oestreich, *J. Am. Chem. Soc.*, 2017, **139**, 16334–16342; (*d*) H. F. T. Klare, M. Oestreich, J.-i. Ito, H. Nishiyama, Y. Ohki and K. Tatsumi, *J. Am. Chem. Soc.*, 2011, **133**, 3312–3315; (*e*) F. Forster, V. M. R. Lopez and M. Oestreich, *J. Am. Chem. Soc.*, 2018, **140**, 1259–1262.

12 (*a*) J. Weismann, R. Waterman and V. H. Gessner, *Chem.–Eur. J.*, 2016, **22**, 3846–3855; (*b*) J. Weismann, L. T. Scharf and V. H. Gessner, *Organometallics*, 2016, **35**, 2507–2515.

13 L. T. Scharf, J. Weismann, K.-S. Feichtner, F. Lindl and V. H. Gessner, *Chem.–Eur. J.*, 2018, **24**, 3439–3443.

14 (*a*) C. P. Casey, S. W. Singer, D. R. Powell, R. K. Hayashi and M. Kavana, *J. Am. Chem. Soc.*, 2001, **123**, 1090–1100; (*b*) L. Korean-Selfridge, H. N. Londino, J. K. Vellucci, B. J. Simmons, C. P. Casey and T. B. Clark, *Organometallics*, 2009, **28**, 2085–2090.

15 (*a*) M. W. Drover, L. L. Schafer and J. A. Love, *Angew. Chem., Int. Ed.*, 2016, **55**, 3181–3186; (*b*) M. W. Drover, E. G. Bowes, J. A. Love and L. L. Schafer, *Organometallics*, 2017, **36**, 331–341.

16 M. A. Rankin, K. D. Hesp, G. Schatte, R. McDonald and M. Stradiotto, *Dalton Trans.*, 2009, 4756–4765.

17 (*a*) G. Durgaprasad, J. A. Luna, K. D. Spielvogel, C. Haas, S. K. Shaw and S. R. Daly, *Organometallics*, 2017, **36**, 4020–4031; (*b*) K. D. Spielvogel, J. A. Luna, S. M. Loria, L. P. Weisburn, N. C. Stumme, M. R. Ringenberg, G. Durgaprasad, J. M. Keith, S. K. Shaw and S. R. Daly, *Inorg. Chem.*, 2020, **59**, 10845–10853.

18 B. Pan, M. W. Bezpalko, B. M. Foxman and C. M. Thomas, *Organometallics*, 2011, **30**, 5560–5563.

19 (*a*) Md. Zafar, R. Ramalakshmi, A. Ahmad, P. K. S. Antharjanam, S. Bontemps, S. Sabo-Etienne and S. Ghosh, *Inorg. Chem.*, 2021, **60**, 1183–1194; (*b*) M. Zafar, A. Ahmad, S. Saha, R. Rongala, T. Roisnel and S. Ghosh, *Chem. Sci.*, 2022, **13**, 8567–8575; (*c*) M. Zafar, R. Ramalakshmi, K. Pathak, A. Ahmad, T. Roisnel and S. Ghosh, *Chem.–Eur. J.*, 2019, **25**, 13537–13546; (*d*) A. Ahmad, S. Saha, M. Zafar, T. Roisnel, P. Ghosh and S. Ghosh, *Eur. J. Org Chem.*, 2023, **989**, e202201283.

20 (*a*) S. Saha, A. Haridas, F. Assanar, C. Bansal, P. K. S. Antharjanam and S. Ghosh, *Dalton Trans.*, 2022, **51**, 4806–4813; (*b*) S. Saha, F. Assanar, A. Ahmad, A. Bains, S. Nagendran and S. Ghosh, *Organometallics*, 2024, **43**, 718–725.

21 (*a*) S. Ye, B. Sarkar, C. Duboc, J. Fiedler and W. Kaim, *Inorg. Chem.*, 2005, **44**(8), 2843–2847; (*b*) M. K. Biswas, S. C. Patra, A. N. Maity, S. C. Ke, N. D. Adhikary and P. Ghosh, *Inorg. Chem.*, 2012, **51**, 6687–6699.

22 (*a*) F. Chen, G. –F. Wang, Y. –Z. Li, X. –T. Chen and Z. –L. Xue, *Inorg. Chem. Commun.*, 2012, **21**, 88–91; (*b*) D. O'Hare, J. C. Green, T. P. Chadwick and J. S. Miller, *Organometallics*, 1988, **7**, 1335–1342; (*c*) P. G. Gass man, J. W. Mickelson and J. R. Sowa Jr, *J. Am. Chem. Soc.*, 1992, **114**, 6942–6944.

23 K. E. Rosenkoetter, M. K. Wojnar, B. J. Charette, J. W. Ziller and A. F. Heyduk, *Inorg. Chem.*, 2018, **57**, 9728–9737.

24 N. L. Fry, M. J. Rose, C. Nyitray and P. K. Mascharak, *Inorg. Chem.*, 2008, **47**, 11604–11610.

25 (*a*) S. Kundu, D. Dutta, S. Maity, T. Weyhermuller and P. Ghosh, *Inorg. Chem.*, 2018, **57**, 11948–11960; (*b*) N. P. V. Leest, M. A. Tepaske, J. H. Oudsen, B. Venderbosch, N. R. Rietdijk, M. A. Siegler, M. Tromp, J. I. V. D. Vlugt and B. D. Bruin, *J. Am. Chem. Soc.*, 2020, **142**, 552–563; (*c*) H. Masui, A. B. P. Lever and P. R. Auburn, *Inorg. Chem.*, 1991, **30**, 2402–2410; (*d*) S. D. J. McKinnon, B. O. Patrick, A. B. P. Lever and R. G. Hicks, *Chem. Commun.*, 2010, **46**, 773–775.

26 (*a*) M. A. Esteruelas, I. Fernandez, A. M. Lopez, M. Mora and E. Onate, *Organometallics*, 2012, **31**, 4646–4649; (*b*) M. L. Buil, M. A. Esteruelas, K. Garces and E. Onate, *J. Am. Chem. Soc.*, 2011, **133**, 2250–2263.

27 (*a*) K. Saha, D. K. Roy, R. D. Dewhurst, S. Ghosh and H. Braunschweig, *Acc. Chem. Res.*, 2021, **54**, 1260–1273; (*b*) K. Pathak, S. Mishra, C. Nandi, S. Saha and S. Ghosh, *Inorg. Chem.*, 2023, **62**, 160–169.

28 (*a*) M. R. St.-J. Foreman, A. F. Hill, G. R. Owen, A. J. P. White and D. J. Williams, *Organometallics*, 2003, **22**, 4446–4450; (*b*) G. R. Owen, *Chem. Soc. Rev.*, 2012, **41**, 3535–3546; (*c*) R. J. Abernethy, A. F. Hill, N. Tshabang, A. C. Willis and R. D. Young, *Organometallics*, 2009, **28**, 488–492; (*d*) M. Jiménez-Tenorio, M. C. Puerta and P. Valerga, *Organometallics*, 2009, **28**, 2787–2798.

29 (*a*) R. Ramalakshmi, K. Saha, D. K. Roy, B. Varghese, A. K. Phukan and S. Ghosh, *Chem.–Eur. J.*, 2015, **21**, 17191–17195; (*b*) K. Pathak, S. Gayen, S. Saha, C. Nandi, S. Mishra and S. Ghosh, *Chem.–Eur. J.*, 2022, **28**, e202104393; (*c*) S. Gayen, S. Shyamal, S. Mohapatra, P. K. S. Antharjanam and S. Ghosh, *Chem.–Eur. J.*, 2023, **30**, e202302362.

30 (*a*) M. L. Buil, J. J. F. Cardo, M. A. Esteruelas, I. Fernandez and E. Onate, *Organometallics*, 2015, **34**, 547–550; (*b*) J. C. Babon, M. A. Esteruelas, I. Fernandez, A. M. Lopez and E. Onate, *Inorg. Chem.*, 2018, **57**, 4482–4491; (*c*) M. A. Esteruelas, F. J. Fernandez-Alvarez, A. M. Lopez, M. Mora and E. Onate, *J. Am. Chem. Soc.*, 2010, **132**(16), 5600–5601; (*d*) M. A. Esteruelas, I. Fernandez, C. García-Yebra, J. Martín and E. Onate, *Organometallics*, 2017, **36**(12), 2298–2307.

31 N. Arnold, S. Mozo, U. Paul, U. Radius and H. Braunschweig, *Organometallics*, 2015, **34**, 5709–5715.

32 V. Lyaskovskyy and B. Bruin, *ACS Catal.*, 2012, **2**, 270–279.

33 V. Montiel-Palma, M. Lumbierres, B. Donnadieu, S. Sabo-Etienne and B. Chaudret, *J. Am. Chem. Soc.*, 2002, **124**, 5624–5625.